ACS APPLIED MATERIALS & INTERFACES

FORUM ARTICLE

www.acsami.org

Covalent Binding of Single-Walled Carbon Nanotubes to Polyamide Membranes for Antimicrobial Surface Properties

Alberto Tiraferri,[†] Chad D. Vecitis,[‡] and Menachem Elimelech*,[†]

[†]Department of Chemical and Environmental Engineering, Yale University, P.O. Box 208286, New Haven, Connecticut 06520-8286, United States

[‡]School of Engineering and Applied Sciences, Harvard University, Cambridge, Massachusetts 02138, United States

Supporting Information

ABSTRACT: We propose an innovative approach to impart nanomaterial-specific properties to the surface of thin-film composite membranes. Specifically, biocidal properties were obtained by covalently binding single-walled carbon nanotubes (SWNTs) to the membrane surface. The SWNTs were first modified by purification and ozonolysis to increase their sidewall functionalities, maximize cytotoxic properties, and achieve dispersion in aqueous solution. A tailored reaction protocol was developed to exploit the inherent moieties of hand-cast polyamide membrane surfaces and create covalent amide bonds with the functionalized SWNTs. The reaction is entirely aqueous-based and entails activation of the carboxylate groups of both the membrane and the nanomaterials to maximize reaction with ethylenediamine. The presence of SWNTs was verified after sonication of the membranes, confirming the strength of the bond between the SWNTs and the membrane surface. Characterization of the SWNT-functionalized surfaces demonstrated the attainment of membranes with novel properties that continued to exhibit high performance in water separation processes. The presence of surface-bound antimicrobial SWNTs was confirmed by experiments using *E. coli* cells that demonstrated an enhanced bacterial cytotoxicity for the SWNT-coated membranes. The SWNT membranes were observed to achieve up to 60% inactivation of bacteria attached to the membrane within 1 h of contact time. Our results suggest the potential of covalently bonded SWNTs to delay the onset of membrane biofouling during operation.

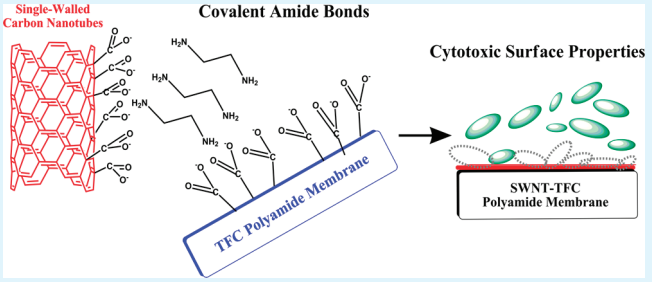

KEYWORDS: polyamide membranes, biofouling, single-walled carbon nanotubes, SWNT, SWCNT, thin-film composite, surface modification, water purification, amide bonds, nanocomposite, biocidal membrane

INTRODUCTION

Membrane-based water separation processes utilize semipermeable membranes to retain contaminants. The surface of the membranes is in contact with feedstreams that carry dissolved molecules, particulates, and microorganisms that can induce membrane fouling.[1] Biofouling, the growth of a biofilm on membrane surfaces, results in a decrease in membrane performance, which, in turn, increases the overall energy requirement of the separation process and decreases membrane life.[1,2] Thus, biofouling control is one of the most pressing challenges faced by the membrane science community. This challenge can be overcome by the use of well-designed functional materials that prevent attachment or growth of microorganisms at the membrane surface, while maintaining high separation performance during operation.

Thin-film composite (TFC) membranes represent the state-of-the-art in dense separation membranes such as those used in reverse osmosis. The active layer of these membranes is in contact with the feed solution and separates water from contaminants through a solution-diffusion mechanism.[3] Decades of research and development, both in industry and academia, have resulted in the success of aromatic polyamide TFC membranes. Currently, polyamide is the benchmark material for the TFC membrane active layer, showing unrivaled productivity and selectivity performance and a high degree of tunability.[4] However, one major drawback of polyamide is its degradation in the presence of chemical oxidants,[4,5] which are normally used to control microbial growth. Thus, alternatives to these degradative oxidants must be considered. To address this challenge, methods to functionalize the active layer have been proposed as solutions to reduce and/or delay polyamide membrane biofouling.

Efforts toward membrane active layer modification have focused on rendering the surface more hydrophilic, smooth, and less charged.[4,6] Examples include the production of novel polyamide-based materials with tailored chemistry and morphology achieved by the addition of monomers or variation of conditions during interfacial polymerization.[7,8] However, the unsurpassed separation properties of polyamide limit the range of improvements that can be made following this pathway. Other studies have investigated modifications of the thin film

Received: May 1, 2011
Accepted: June 13, 2011
Published: June 30, 2011

dx.doi.org/10.1021/am200536p | ACS Appl. Mater. Interfaces 2011, 3, 2869–2877

interface by postfabrication procedures, such as employing surface coating techniques established in polymeric materials research. These methods entail attachment of hydrophilic or antimicrobial macromolecules via graft polymerization,[9,10] free radical polymerization,[11] or coating by deposition.[12−15] Results obtained using the previously stated, macromolecule-based procedures suggest that progress toward the prevention of fouling and biofouling will be limited and call for a paradigm shift in antifouling membrane design.[6]

The functionalization of thin-film membranes with active nanomaterials may be a novel strategy to tailor membrane antifouling characteristics. Nanomaterial-specific properties can be imparted to the membrane by creating nanocomposite structures or coating the membrane with the nanomaterial. Incorporation of nanoparticles within the polymeric film during interfacial condensation is the route used for thin-film nanocomposite membranes. For example, silver nanoparticles,[16] titanium oxide[17] nanoparticles, and silver-exchange zeolites[18] have been employed to yield membranes with enhanced antimicrobial properties. One drawback of this type of modification is that incorporation of nanomaterials during polymerization also affects the polymer chemistry and, in turn, the thin film separation performance in ways that are difficult to predict. Furthermore, the majority of the nanomaterial mass is buried in the bulk polymer and thus, the active nanomaterial surface is rendered useless. Postfabrication functionalization may be a more effective option for improved control of nanomaterial spatial localization. Recent studies in this direction have proposed strategies to modify the polyamide thin film surfaces with TiO_2 nanoparticles,[19−21] which under UV irradiation were observed to exhibit antimicrobial activity.

Single-walled carbon nanotubes (SWNTs) have been proposed as antimicrobial agents for a variety of environmental applications.[22] Although the mechanism of toxicity is still not fully understood, recent studies suggest a combination of cell membrane perturbation and oxidative stress as the main cause of bacterial inactivation.[23] The physicochemical mechanism of toxicity provided by SWNTs ensures inactivation of a broad range of microorganisms,[24] without stimulating antibiotic resistance.[22] Furthermore, SWNTs can be used as stand-alone nanomaterials, as opposed to titanium dioxide nanoparticles, which require UV irradiation to ensure adequate bacterial inactivation.[19,20] Finally, SWNTs represent nondepleting biocides, as the related toxicity process does not involve the leaching of ionic or chemical species from the bulk of the nanomaterials, as in the case of silver nanoparticles.[25−28]

In this study, we propose a novel approach to impart nanomaterial-specific properties to the active surface of thin-film composite (TFC) polyamide membranes. In particular, antimicrobial properties were conferred to polyamide membranes by covalently binding cytotoxic single-walled carbon nanotubes to their surfaces. Our results suggest the potential of these membranes to delay the onset of biofouling in membrane-based separation applications, as well as the promise of the proposed functionalization platform in a variety of other systems requiring reactive surfaces.

MATERIALS AND METHODS

Materials and Chemicals. *N*-(3-Dimethylaminopropyl)-*N*′-ethylcarbodiimide hydrochloride (EDC, 98%), N-hydroxysuccinimide (NHS, 98%), ethylenediamine (ED, BioXtra), HEPES (>99.5%), MES monohydrate (>99.0%, BioXtra), *N*,*N*-dimethylformamide (DMF, anhydrous, 99.8%), 1-methyl-2-pyrrolidinone (NMP, anhydrous, 99.5%), dimethyl sulfoxide (DMSO, 99.5%), 1,3-phenylenediamine (MPD, >99%), 1,3,5-benzenetricarbonyl trichloride (TMC, 98%), and phosphate buffered saline (PBS, BioReagent) were used as received (Sigma-Aldrich, St. Louis, MO). Sodium chloride (NaCl, crystals, ACS reagent) from J.T. Baker (Phillipsburg, NJ) was used to adjust ionic strength of the reacting solutions and for the membrane performance evaluation. The pH of the reacting solutions was adjusted using hydrochloric acid (HCl) or sodium hydroxide (NaOH). Propidium iodide (PI) and 4′,6-diamidino-2-phenylindole (DAPI) were purchased from Invitrogen (Carlsbad, CA). Unless specified, all chemicals were dissolved in deionized (DI) water obtained from a Milli-Q ultrapure water purification system (Millipore, Billerica, MA).

Single-walled carbon nanotubes (SWNTs, lot number SG65−000−0031), produced by the CoMoCAT process, were obtained from SouthWest NanoTechnologies, Inc. (Norman, OK). Manufacturer specifications of the SWNTs include: tube diameter of 0.8 ± 0.1 nm, carbon content >90% by weight, >50% of tubes are (6,5) chirality, and >90% of tubes are semiconducting.

Thin-Film Composite Polyamide Membranes. TFC membranes were prepared by interfacial polymerization of polyamide onto commercial polysulfone (PSf) ultrafiltration membranes (PS20, Sepro Membranes, Oceanside, CA), adapting a procedure described in our previous publication.[29] The PSf support was immersed in a 3.4 wt % aqueous MPD solution for 120 s, and an air knife was used to remove the excess solution from the membrane surface. Next, the MPD-saturated support membrane was immersed for 60 s in a 0.15 wt % TMC in Isopar G, a nonpolar organic solvent (Univar, Redmond, WA), to form the ultrathin PA layer by interfacial polymerization. Chemicals used for post-treatment of the polyamide were sodium hypochlorite (NaOCl, available chlorine 10−15%, Sigma-Aldrich) and sodium bisulfite ($NaHSO_3$, Sigma-Aldrich).

SWNT Purification and Functionalization. As-received SWNTs were purified by heating in concentrated hydrochloric acid (37%) for 12 h at 70 °C. The SWNTs were then rinsed repeatedly with DI water until neutral pH was attained. Amorphous carbon was removed from the SWNTs by oxidation at 350 °C for 6 h. Treatment of SWNTs by ozone was used for generating sidewall defects to facilitate functionalization, reduce the length of the nanotubes, and enhance dispersion in aqueous solution.[30−32] Approximately 5 mg of purified SWNTs were sonicated for 1 h in 20 mL of DMF. Mats of SWNTs were then prepared by filtering the suspension through a 5-μm Omnipore PTFE membrane (Millipore) to form a SWNT film. At least 100 mL of ethanol were then filtered through the SWNT-coated filter to remove residual solvent, followed by an extensive wash with DI water to remove residual ethanol. After air-drying the SWNT-coated filter, it was placed in a UV/O_3 generator in ambient laboratory air for 10 h (BioForce Nanosciences, Inc., Ames, IA).

SWNT Characterization. Raman spectra were acquired utilizing an excitation wavelength of 532 nm on a WITec CRM 200 Spectrophotometer. Thermogravimetric analysis (TGA) (SETSYS 16/18) was performed from 200 to 1000 °C at a heating rate of 10 °C/min. X-ray photoelectron spectroscopy (XPS, Thermo Scientific ESCALAB 250) and transmission electron microscopy (TEM, FEI Titan 80−300) of SWNTs were conducted at CAMCOR (University of Oregon, Eugene, OR).

SWNT-Polyamide Membrane Surface Reaction. Scheme 1 describes the protocol for covalent binding of SWNTs to the PA surface to create SWNT-TFC membranes. All reaction chemistry was completed in an aqueous solution. A 7-cm diameter TFC membrane was loaded into a custom-made dead-end filtration unit with only the active (top) surface accessible. The dead-end filtration unit is made of stainless steel and equipped with a built-in magnetic stir bar. EDC (4 mM) and NHS (10 mM) were dissolved in 125 mL of 0.5 M NaCl solution buffered at pH 5 (MES), and the solution was put in contact with the membrane surface for 1 h (Step 1A-B of Scheme 1). During this step, the native carboxylate groups of the polyamide surface were converted into intermediate amine-reactive esters for cross-linking.[33,34] The activated esters were used promptly for reaction with ethylenediamine (ED) to form amide bonds by contacting the membrane surface with a 125-mL

Scheme 1. Procedure to Covalently Bind SWNTs to the Membrane Surface[a]

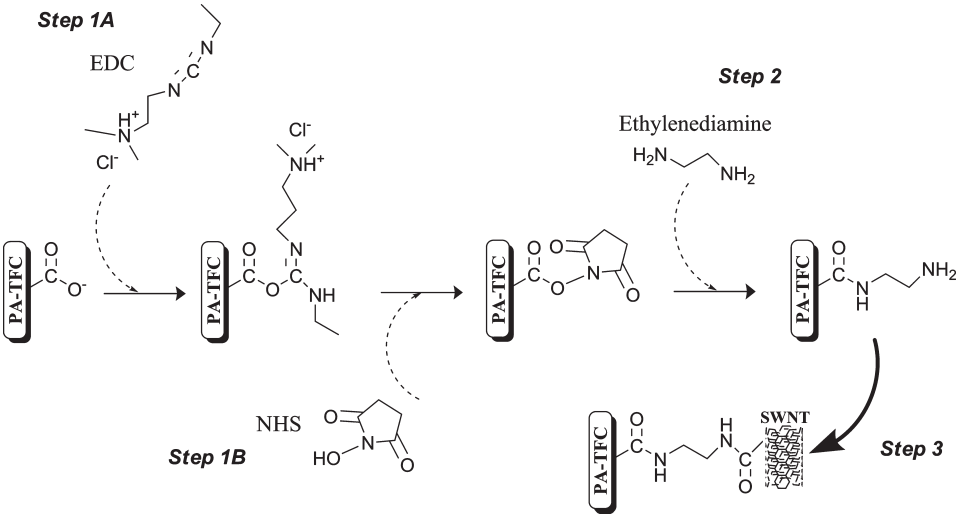

[a] The native carboxylic groups of the polyamide active film are converted into semistable amine-reactive esters using an EDC/NHS solution at pH 5 (MES buffer), followed by reaction with ethylenediamine at pH 7.5 (HEPES buffer) and contact with a sonicated suspension of functionalized SWNTs in the presence of EDC/NHS.

solution of 10 mM ED and 0.15 M NaCl buffered at pH 7.5 (HEPES) for 30 min (Step 2 of Scheme 1).

Approximately 10 mg of ozonized SWNTs were dispersed in 250 mL of solution at pH 7 (HEPES and NaOH) by high-power probe sonication (40 W, Sonicator 3000, Misonix Inc., Farmingdale, NY) for 3 h. EDC and NHS were then dissolved in the sonicated suspension at concentrations of 4 and 10 mM, respectively. The resulting solution was added to the filtration chamber to initiate tethering of SWNTs to the amine groups at the membrane surface (Step 3 of Scheme 1). Constant stirring was provided and a pressure of 50 psi (13.8 bar) was applied to facilitate contact between the SWNTs and the membrane surface. Reaction was carried out at room temperature (23 °C) for 3 h. Aggregation of the SWNT bundles during this reaction time was ruled out, based on dynamic light scattering measurements of SWNT hydrodynamic diameter carried out for 45 min under the same conditions as those used for the reaction. The measured hydrodynamic radius of the SWNTs was 540 ± 38 nm and remained constant during the experiment.

After the reaction, the SWNT suspension was discarded and the membrane surface was briefly contacted with a solution at pH 11 (NaOH) to restore the unreacted carboxylic groups. Finally, the membrane surface was rinsed thoroughly with DI water. The strength of the covalent bonds between SWNTs and the surface of the membranes was challenged by subjecting the SWNT-TFC membranes to two 7-min cycles of bath sonication (FS60, Fisher Scientific Co., Pittsburgh, PA).

Membrane Characterization. Pure water permeability, A, and NaCl permeability, B, of the hand-cast membranes were evaluated in a dead-end filtration unit before and after reaction with the SWNTs, following procedures described in our previous publication.[29] The loaded membrane (area was 38.5 cm^2) was first compacted with DI water at an applied pressure of 100 psi (27.6 bar) until the permeate flux reached a steady state. Salt rejection was characterized by keeping the same applied pressure and measuring rejection of 20 mM NaCl solution using a calibrated conductivity meter (Oakton Instruments, Vernon Hills, IL). All experiments were carried out at a fixed temperature of 23 °C.

Membrane characterization was performed on polyamide films as cast, and on SWNT-TFC membranes before and after the bath sonication protocol described above. Membrane surface roughness was analyzed using a Multimode AFM (Veeco Metrology Group, Santa Barbara, CA) in tapping mode. Symmetric silicon probes with 30-nm-thick back side aluminum coating were employed (Tap300A, Bruker Nano Inc., Camarillo, CA). The probe had a spring constant of 40 N/m, resonance frequency of 300 kHz, tip radius of 8 ± 4 nm, and cantilever length of 125 ± 10 μm. Air-dried membranes were scanned in air at 10 randomly selected scan positions. The surface roughness of each membrane was quantified as the root-mean-square (rms) roughness, average roughness R_a, maximum roughness R_{max}, and surface area difference (SAD, determined by dividing the actual surface area by the planar area).

Surface hydrophilicity was evaluated from DI water contact angle measurements using the sessile drop method (VCA Video Contact Angle System, AST Products, Billerica, MA). The system is equipped with software to determine the left and right contact angles (VCA Optima XE). To account for variations between different measurements on the same surface, several desiccator-dried samples were tested in eight random locations. The highest and the lowest equilibrium angles were discarded and the remaining data were averaged. The relative wettability of the membranes was evaluated by calculating the solid−liquid interfacial free energy adjusted for roughness by incorporating the surface area difference, SAD, determined from AFM measurements[35,36]

$$-\Delta G_{SL} = \gamma_L\left(1+\frac{\cos\theta}{SAD}\right)$$

where θ is the average contact angle and γ_L is the pure water surface tension (72.8 mJ/m^2 at 25 °C).

Surface morphology of membranes was visualized by scanning electron microscopy, SEM (FEI XL-30 ESEM). The desiccator-dried membranes were sputter-coated with gold and analyzed at a voltage of 10 kV. The thin film of the membranes was analyzed using TGA. To prepare the samples for TGA measurements, membranes were placed in NMP for 30 min to dissolve the underlying PSf. Once the support layer was completely dissolved, the top active layer was collected and dried overnight at 65 °C to volatilize the residual NMP.

Evaluation of Antibacterial Activity of SWNTs and of SWNT Functionalized Membranes. *Escherichia coli* (*E. coli*) K12 MG1655 was used as the model bacteria. The *E. coli* cells were incubated in Luria−Bertani (LB) broth with 50 mg/L kanamycin at 37 °C and harvested at midexponential growth phase. The bacterial suspension was washed three times by centrifugation (Sorvall SS-34) at 15 000 rpm for 3 min and

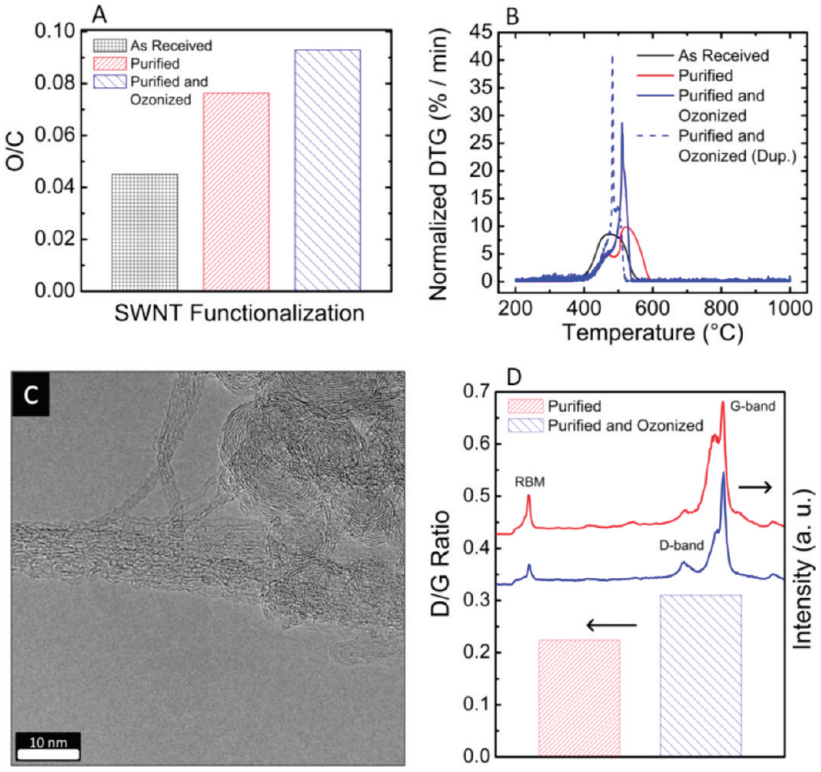

Figure 1. Characteristics of the SWNTs. (A) Oxygen to carbon ratio as obtained by X-ray photoelectron spectroscopy (XPS) analysis for the as-received (black), purified (red), and ozonized (blue) SWNTs. (B) Differential thermogravimetric (DTG) plots normalized to the total initial mass of sample for the as-received (black), purified (red), and ozonized SWNTs in duplicate (solid and dashed blue curves). (C) Representative TEM micrograph of the ozonized SWNTs showing bundles of single-walled carbon nanotubes. (D) Raman spectra acquired using 532 nm excitation and relative D/G ratio for the purified (red) and ozonized (blue) SWNTs.

resuspended in an isotonic saline solution (0.9% NaCl) to remove residual macromolecules and other growth medium constituents.

To evaluate SWNT cytotoxicity, we used a SWNT-coated filter assay.[23,37] Briefly, ozonized carbon nanotubes were dispersed in DMSO at a concentration of 0.1 to 0.2 mg/mL using a 15-min probe sonication. SWNT-coated filters were then prepared following the protocol described earlier in this paper. To facilitate direct contact between the SWNT mat and the bacteria, *E. coli* cells (1×10^7 cells/mL) were gently deposited by vacuum filtration onto the SWNT-coated filters. After a 1-h incubation, the cells were stained with PI for 15 min, and then counterstained with DAPI for 5 min in the dark. Fluorescence images were then taken under an epifluorescence microscope (Olympus BX40) with a U filter (excitation 364 nm/emission 440 nm) for detecting cells stained with both PI and DAPI, and with an IB filter (excitation 464 nm/emission 604 nm) for detecting cells stained with PI. Ten representative images were taken at 10X magnification at various locations. Dead cells and the total number of cells were determined by direct cell counting on the SWNT-coated filter. The percentage of dead cells (or loss of viability) was determined from the ratio of the number of cells stained with PI divided by the total number of cells.

To evaluate inactivation of bacteria by the SWNT functionalized membranes, a plate counting method was adopted. Control membranes and sonicated SWNT-TFC membranes were attached to a glass plate using laboratory tape, with only the active surface accessible to solution. *E. coli* cells (1×10^7 cells/mL) were pipetted onto the surfaces using approximately 0.5 mL of suspension per 1 cm^2 of membrane. The cell-covered surfaces were then incubated for 1 h at 23 °C under gentle stirring. After this time, the excess bacterial suspension was discarded and two 1-in. coupons were punched for each sample. The samples were rinsed extensively with PBS and each coupon was placed in a 50-mL Falcon tube containing 10 mL of PBS solution. The Falcon tubes were then immersed in water and gently bath sonicated for 7 min. This procedure was observed to resuspend bacterial cells from surfaces without affecting their viability,[38] which was confirmed in our laboratory (data now shown). The PBS suspensions of cells were spread on solid LB agar growth plates with kanamycin. In addition, the sonicated coupons were also rinsed with PBS solution and gently tapped on LB agar plates in 5 different locations to account for live cells that were not resuspended during sonication. The colonies formed after 12 to 16 h incubation at 37 °C were counted. The number of colonies counted from the SWNT-TFC surfaces was normalized by the coupon area and by the number of live cells counted from PA control membranes. The procedure was repeated for 3 separately cast and modified membranes. In different experiments, bacteria were not resuspended from PBS-rinsed coupons. Instead, cells were fixed with ~3% glutaraldehyde, sputter-coated with gold, and then viewed under an SEM.

RESULTS AND DISCUSSION

SWNT Characteristics. Short, highly functionalized, and debundled SWNTs exhibit enhanced antibacterial activity, due to their enhanced dispersivity in aqueous solution and the larger contact area with the bacterial cells.[39−41] In this study, ozonolysis was employed to shorten and functionalize the nanotubes before they were reacted with the membranes. Previous studies have shown that ozone can preferentially attack the defect sites at the nanotubes walls,[42] thereby creating carboxylic functional groups,[31,32,43] reducing particle size,[31,43] enhancing dispersion in water,[43] and maximizing the O/C ratio.[32,43]

XPS data (Figure 1A) demonstrated an increase in the O/C ratio for the ozonized sample compared to the as-received or purified

SWNTs. This observation indicates a higher amount of oxidized carbon to elemental carbon and a higher density of oxygen-rich functional groups. It is likely that the short-lived ozonide intermediates formed during ozonation are converted into carboxylic acids in the presence of UV irradiation and atmospheric moisture.[30,32]

Raman analysis of the purified and ozonized SWNTs is presented in Figure 1D. The diameter-dependent frequency of the radial breathing mode (RBM) appeared at a wavenumber of ν 276 cm^{-1} for both samples. The tube diameter, d, was estimated from the RBM[37,44] ($d = 248/\nu$), yielding a value of approximately 0.9 nm, consistent with the manufacturer specifications. The ratio between the SWNT disorder-induced D-band (1320 cm^{-1}) and the tangential mode G-band (1585 cm^{-1}) is an empirical measure of the sample purity and number of defects.[44] This ratio was higher for the ozonized sample, indicating that the functionalization process increased the concentration of defects and of sp^3-hybridized carbon atoms on the SWNT sidewalls.[30,45] The increase in the D/G ratio measured by Raman was similar to the increase in the O/C ratio obtained by XPS, suggesting that the increased defect density observed by Raman was correlated to the oxidation of the nanotube sidewalls.[32]

The findings from the XPS and Raman analyses were confirmed by thermogravimetric analysis. DTG plots (Figure 1B) show sharpening and shifting of the mass loss peak to a lower temperature for the ozonized SWNTs (blue) with respect to the purified SWNTs (red). This result is representative of the production of sp^3-oxy functional groups that reduce the oxidative stability of the SWNTs,[46] and of the presence of a greater number of sidewall defects that causes the nanotubes to combust at a lower threshold temperature.[47]

Representative TEM micrographs of ozonized SWNTs (Figure 1C) confirmed that nanotubes were single-walled and that their sidewall structure remained intact after treatment. Negligible metal impurities and amorphous carbon were visible. TGA data (see Figure S1 in the Supporting Information) indicated that the purification and functionalization procedures decreased the concentration of residual metal impurities from 4.3% for the as-received to 2.2% and 2.1% for the purified and ozonized SWNTs, respectively.

Antibacterial Properties of SWNTs. *E. coli* K12 was used to evaluate the SWNT cytotoxicity. Bacteria in direct contact with SWNT-coated filters were incubated for 1 h at 37 °C. The bacteria-coated SWNT filters were then stained and viability loss was determined by fluorescence microscopy. The percent loss of *E. coli* viability for the purified and ozonized SWNTs was >95% and significantly higher than that of the purified-only carbon nanotubes (~80%). The results are in agreement with previous studies on the antibacterial properties of SWNTs.[23,37,40,41] SWNT antimicrobial activity requires direct contact with the bacterial cells, and the cytotoxic effects involve a combination of cell membrane perturbation and oxidative stress.[23,40,48] The observed cytotoxic properties of SWNTs correlated with the extent of ozonolysis treatment, as shown in Figure S2 of the Supporting Information.

Membrane Surface Characteristics. The hand-cast thin-film polyamide membranes possess native surface carboxylate groups resulting from incomplete reaction and hydrolysis of the TMC acyl halides during interfacial polymerization.[49] These reactive moieties were utilized as SWNT binding sites, following the reaction procedure delineated earlier in this paper. During reaction, covalent cross-linking between the carboxylic groups at the membrane surface and at the SWNT walls occurred via amide bond formation with ethylenediamine (Scheme 1).[45,50−52]

Visual inspection of the membranes before and after reaction with SWNTs yields insight into the extent of nanomaterial attachment. Figure S3 in the Supporting Information shows digital images of active layer surfaces and oven-dried thin films for the control and SWNT-TFC membranes. Surface functionalization was apparent through the darkening of the membrane upon reaction, suggesting a significant presence of tightly anchored SWNTs even after membrane sonication. Ultrasonication resulted in the removal of the loosely bound nanomaterials and the larger SWNT bundles and aggregates. The anchored SWNTs that were able to endure sonication suggest an irreversible functionalization of the membrane surface.

The amount of SWNTs on a sonicated SWNT-TFC membrane was estimated by gravimetric analysis to be approximately 7 wt % of the total thin film, equivalent to a total SWNT loading of 0.03 mg/cm^2 on the functionalized membrane (see Figure S4 in the Supporting Information). TGA measurements performed on the thin films collected after PSf dissolution showed a shift in the material thermal degradation peak to a lower temperature (see Figure S4 in the Supporting Information). A lower thermal stability suggests that the presence of SWNTs may decrease the intermolecular bonding and the aromaticity of polyamide during sample preparation,[53,54] and possibly accelerate the diffusion of oxygen and volatile thermo-oxidative products between the gas phase and the bulk polymer.[55]

Figure 2 presents representative SEM micrographs and AFM images of control membranes and sonicated SWNT-TFC membranes. Roughness data from AFM analysis is also reported. The representative topographic image (Figure 2A) and SEM surface micrograph (Figure 2C) of a control membrane show a uniform ridge-and-valley morphology, which is typical of polyamide thin films formed by interfacial condensation.[4] The membrane surface roughness (rms = 42.2 ± 12.9 nm) was at the lower end of the range observed for commercial reverse osmosis polyamide membranes.[15] The film thickness can be estimated from the roughness data (~300 nm), a value characteristic of layers cast under similar conditions.[56]

Significant differences were observed via AFM for the functionalized SWNT-TFC membranes as compared to the unmodified membranes. The ridge-and-valley morphology appeared more leveled and at times completely flattened. Furthermore, bulkier features were detected that correlated well with the size of the larger SWNT aggregates measured by DLS. Figure 2B is a representative image displaying some of these characteristics. These changes in membrane morphology are attributed to the presence of SWNTs at the surface. No change in surface roughness was observed after exposing the membranes to only those chemical compounds used during reaction with SWNTs (see Figure S5 in the Supporting Information).

The SEM micrograph in Figure 2D shows that the ridge-and-valley features of the SWNT-TFC membrane surface are overlain by other features of comparable or larger size. These features are assumed to be bundles or aggregates of SWNTs. SWNTs were observed to be scattered and interspersed on the polyamide and may be the reason for the apparent smoother morphology imaged by AFM. Large SWNT aggregates were also observed on the surface, comparable to the larger size features on the membrane surface observed by AFM. More SEM micrographs of the sonicated SWNT-TFC membranes are presented in the Supporting Information (Figure S6). Figure S6 in the Supporting Information also shows SEM surface micrographs of SWNT-TFC membranes before sonication. Very large SWNT

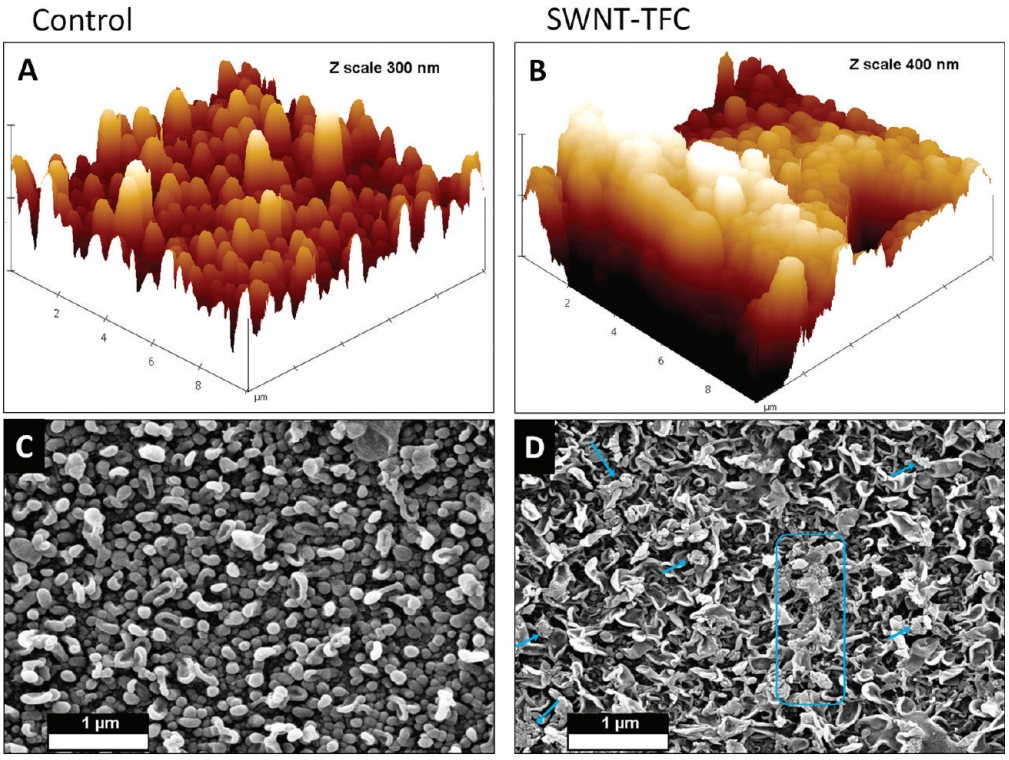

42.2 ± 12.9	**RMS (nm)**	134.9 ± 60.2
33.0 ± 10.3	**R_a (nm)**	103.2 ± 44.8
314 ± 99	**R_{max} (nm)**	940 ± 347
9.2 ± 4.8	**SAD (%)**	18.7 ± 7.9

Figure 2. Imaging by (A, B) AFM and (C, D) scanning electron microscopy of the membrane surface (A, C) before and (B, D) after functionalization. AFM shows the typical ridge-and-valley morphology of polyamide for the control membrane (A), and the smoothening of these ridge-and-valley structures and appearance of larger features for the functionalized membrane (B). These structures are observable in the representative SEM micrographs: the SWNT-reacted membrane (D) shows the presence of bundled SWNTs overlaying the polyamide surface, some of which are highlighted in blue. Roughness parameters are reported at the bottom of the figure.

aggregates were apparent, which detached during bath sonication. The low surface-to-volume ratio of these large aggregates minimizes the density of binding sites between the membrane and SWNTs, which facilitates detachment during ultrasonication.

The higher average roughness of the modified membranes is attributed to the significant increase in the value of R_{max}, which is related to the large SWNT aggregates. However, a comparable value of surface area difference (SAD) to the polyamide control was observed, due to smoothing of the ridge-and-valley features discussed above. From AFM and SEM data analysis, we can conclude that the SWNT coverage of the membrane was heterogeneous on a microscopic scale. These results confirm the complexity and difficulty of dispersing and debundling narrow-diameter single-walled carbon nanotubes in aqueous solutions without the use of surfactants. Future studies should focus on developing methods to achieve more homogeneous functionalization through optimization of nanomaterial dispersion.

Figure 3 presents contact angle data of DI water in contact with the surface of the control, SWNT-TFC, and sonicated SWNT-TFC membranes. The calculated interfacial free energy of the surface water interaction is also presented, which incorporates SAD values to account for surface roughness. Polyamide control membranes had a contact angle of ~70°, consistent with previous studies.[35] The presence of SWNTs on the membrane surface did not significantly affect surface wettability, as the average equilibrium contact angle was within experimental error of the value measured for the control polyamide surface. Consequently, the calculated interfacial free energy of water was comparable for polyamide and for SWNT-TFC surfaces (~ −95 mJ/m^2). The carbon nanotubes become relatively hydrophilic as a result of the functionalization by the ozonolysis treatment. This finding was confirmed by using the same highly functionalized SWNTs to functionalize more hydrophobic polyamide membranes. The same equilibrium contact angle as that presented in Figure 3 was observed after modification of the more hydrophobic membranes (see Figure S7 in the Supporting Information).

Membrane Transport Properties. The pure water permeability coefficient, *A*, and salt permeability coefficient, *B*, were measured for five separately cast and modified membranes, before and after reaction with SWNTs. A small increase in *A* was observed for the SWNT-TFC membranes compared to the

control membranes. A small loss of NaCl rejection was also measured, translating into a small increase in *B* (see Figure S8 in the Supporting Information). Overall, the membrane transport parameters did not change significantly, indicating that postfabrication surface functionalization is a nondestructive route that minimizes performance loss of the polyamide active layer. The relatively small increase in *A* and *B* is attributed to the contact of the membrane with ethylenediamine during reaction, as the same behavior was observed for membranes that were subjected to the same reaction treatment, but in the absence of SWNTs (see Figure S8 in the Supporting Information). Further optimization of the concentration and contact time with ethylenediamine would minimize the impact on membrane transport properties.

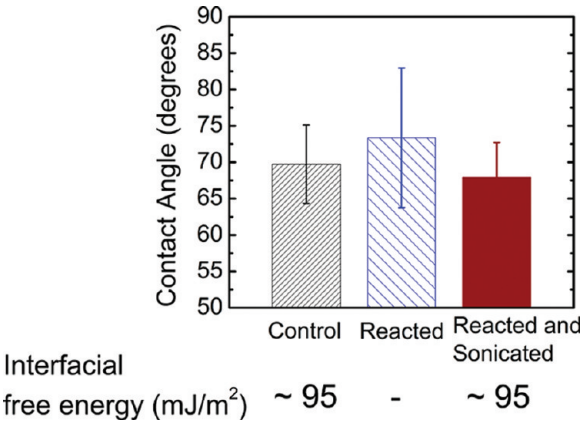

Figure 3. Surface tension and contact angle with deionized water for (black) control, (blue) reacted, and (red) reacted and sonicated membranes. Bars and standard deviations represent the average of six independently cast and functionalized membranes. The average membrane–water interfacial free energy for control polyamide membranes and for membranes that were modified and sonicated was calculated from contact angle and roughness data. The computed value is reported below the plot of contact angle for each respective bar.

Antimicrobial Properties of Membrane Active Layer. The objective of postfabrication functionalization is to confer biocidal functionality to the membrane surface through covalent tethering of SWNTs. The antibacterial activity of the SWNT-TFC membranes was assessed by a plate count assay using *E. coli* as model bacteria. Cells were incubated with the membranes for 1 h in 0.9% NaCl solution, and then resuspended in PBS solution using bath sonication. The suspension was spread on LB agar plates and colonies were counted after overnight incubation. Three functionalized membranes and three control membranes were evaluated. For each membrane tested, a new membrane was cast, and two different 1-in. diameter coupons from each cast membrane were tested independently.

Figure 4B presents the average surface density and standard deviation of culturable cells on the SWNT-TFC membranes, normalized by the number of culturable cells on each respective PA control membrane. The number of culturable bacteria on the SWNT-TFC membranes was significantly lower (~44%) than that on the PA control membranes. Furthermore, the loss of viability of the replicate membrane samples was quite similar, yielding a negligible standard deviation. This result suggests that although membrane functionalization is heterogeneous on the microscale, a statistically comparable amount of cytotoxic SWNTs are available on the surface of the larger size (1-in. diameter) membrane samples utilized for the enumeration of culturable cells.

To validate the culturable bacterial enumeration method by resuspension, the results were compared to experiments where the test membranes were pressed onto agar plates for direct transfer of bacteria. The number of resuspended culturable cells was always at least 2 orders of magnitude greater than the number of live cells counted after contacting the sonicated test coupons on LB agar plates. Live cells still present on the sonicated test coupons were enumerated, and comparable results to those

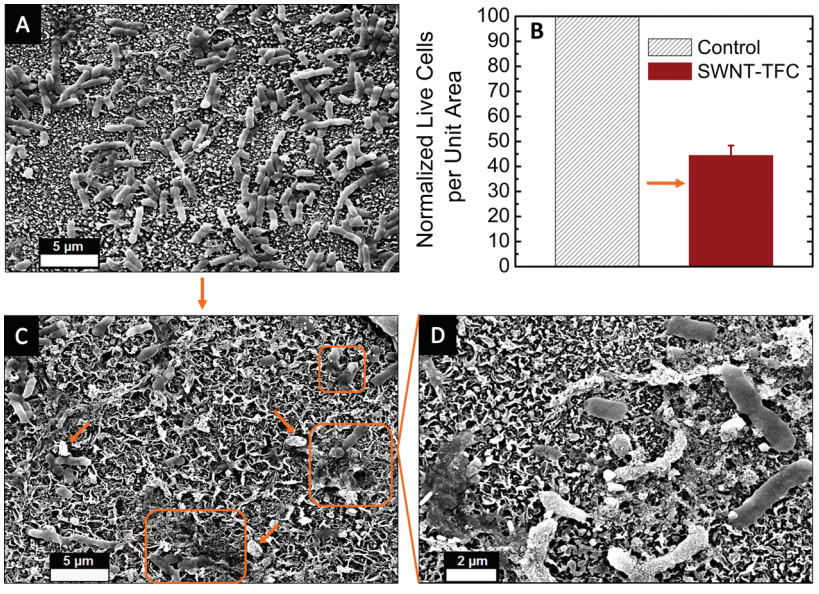

Figure 4. Bacterial inactivation properties of the membrane surface. (B) Colony-forming units enumerated from *E. coli* bacteria resuspended from functionalized SWNT-TFC membranes (red) normalized with those of control membranes (shaded). The tests involved incubation of bacterial suspension in contact with the membrane surface for 1 h in 0.9% NaCl at room temperature (23 °C). Bars with standard deviation represent the average of three separately cast and reacted membranes. The figure presents SEM micrographs displaying *E. coli* at the surface of a (A) control membrane and (C) a SWNT-functionalized membrane at the end of the cytotoxicity test (some cells with lost integrity are highlighted in orange). (D) Magnified view of the surface of a SWNT-TFC membrane with *E. coli* cells: the magnified view is a representative image and does not correspond to the enlargement of micrograph C.

observed from the resuspension assay were obtained. Specifically, 46 ± 15% of live cells were counted on the SWNT-TFC test coupons relative to the PA control coupons. The strong agreement between these two experiments validates the sonication and resuspension assay for enumerating culturable bacteria attached to the membrane surface.

Figure 4 also presents representative SEM images of *E. coli* in contact with control (Figure 4A) and sonicated (Figure 4C,D) SWNT-TFC membrane surfaces after 1 h of incubation in 0.9% NaCl. Viable and dead bacteria showed distinct differences in cell morphology, as shown in past studies of bacteria in contact with SWNTs.[40] Most of the cells on the PA control membranes appeared healthy and their membranes were intact. In contrast, a large number of bacterial cells on the SWNT-TFC sample had lost their membrane integrity. Specifically, the impacted cells appeared either flattened/dehydrated or displayed a compromised cell membrane. The various bacterial morphologies are observable in the higher magnification SEM found in Figure 4D. Additional images of the cells on membrane surfaces are presented in Figure S9 in the Supporting Information. A higher and more homogeneous distribution of SWNTs on the surface would likely enhance the SWNT-TFC membrane surface cytotoxicity.

CONCLUDING REMARKS

In this study, we proposed a methodology for functionalization of surfaces containing native moieties that can be exploited to tether nanomaterials with targeted functionalities. The possibilities for functionalization are virtually limitless, as the variety of nanoparticle interfacial properties and methods to create surface binding sites are vast. This range of platforms represents a remarkable opportunity to target and increase performance of systems requiring specific surface functionalities while maintaining intrinsic properties of the bulk material. In particular, addition of antimicrobial nanomaterials to a membrane surface to increase the availability of their active/reactive surface is a crucial factor in optimizing performance of membrane-based separation systems that are prone to biofouling.

To this purpose, we demonstrated functionalization of dense hand-cast membranes with single-walled carbon nanotubes that were selected for their well documented, nondepleting antimicrobial activity. The biocidal properties of the SWNTs were successfully conferred to the membrane surface upon covalent surface modification. Analysis of the morphological characteristics of the functionalized surfaces suggests that an improved aqueous SWNT dispersion will result in a greater and more homogeneous surface coverage.

ASSOCIATED CONTENT

Supporting Information. Thermogravimetric analysis (TGA) of purified and ozonized SWNTs (Figure S1); *E. coli* inactivation rate by SWNTs as a function of ozonolysis time for both purified SWNTs (Figure S2A) and unpurified SWNTs (Figure S2B); digital images of membrane surfaces (Figure S3A) and dry thin film (Figure S3B); estimation of SWNT loading on sonicated SWNT-TFC membranes and TGA measurements on the thin film of polyamide membranes and SWNT-TFC membranes (Figure S4); surface roughness and representative AFM images of membranes reacted without SWNTs (Figure S5); surface SEM micrographs of control membranes and SWNT-TFC membranes before and after sonication (Figure S6); contact angle of DI water with surface of hand-cast membrane on hand-cast support before and after reaction with SWNTs (Figure S7); transport parameters of membranes before and after reaction with (Figure S8A) and without (Figure S8B) SWNTs; surface SEM micrographs of control membranes and sonicated SWNT-TFC membranes after bacterial cytotoxicity static test (Figure S9). This material is available free of charge via the Internet at http://pubs.acs.org.

AUTHOR INFORMATION

Corresponding Author

*Tel.: +1 (203) 432-2789. Fax: +1 (203) 432-4387. E-mail: menachem.elimelech@yale.edu.

ACKNOWLEDGMENT

We acknowledge the NWRI-AMTA Fellowship for Membrane Technology, awarded to A.T., and the Water-CAMPWS, a Science and Technology Center of Advanced Materials for the Purification of Water with Systems under the National Science Foundation Grant CTS-0120978. We also acknowledge the CAMCOR facilities and technician for XPS and TEM analysis. The CAMCOR TEM Facility is supported by grants from the W. M. Keck Foundation, the M. J. Murdock Charitable Trust, the Oregon Nanoscience and Microtechnologies Institute, the Air Force Research Laboratory (under Agreement FA8650-05-1-5041), and the University of Oregon.

REFERENCES

(1) Ridgway, H. F.; Safarik, J. *Biofouling and Biocorrosion in Industrial Water Systems* **1991**, 81–111.
(2) Herzberg, M.; Elimelech, M. *J. Membr. Sci.* **2007**, *295*, 11–20.
(3) Paul, D. R. *J. Membr. Sci.* **2004**, *241*, 371–386.
(4) Petersen, R. J. *J. Membr. Sci.* **1993**, *83*, 81–150.
(5) Glater, J.; Hong, S. K.; Elimelech, M. *Desalination* **1994**, *95*, 325–345.
(6) Rana, D.; Matsuura, T. *Chem. Rev.* **2010**, *110*, 2448–2471.
(7) Liu, L. F.; Yu, S. C.; Zhou, Y.; Gao, C. J. *J. Membr. Sci.* **2006**, *281*, 88–94.
(8) Liu, M. H.; Yu, S. C.; Tao, J.; Gao, C. J. *J. Membr. Sci.* **2008**, *325*, 947–956.
(9) Kang, G. D.; Liu, M.; Lin, B.; Cao, Y. M.; Yuan, Q. *Polymer* **2007**, *48*, 1165–1170.
(10) Wei, X. Y.; Wang, Z.; Zhang, Z.; Wang, J. X.; Wang, S. C. *J. Membr. Sci.* **2010**, *351*, 222–233.
(11) Niu, Q. J. *Reverse Osmosis Membrane with Branched Poly-(Alkylene Oxide) Modified Antifouling Surface*. U.S.
(12) Wilson, D. R. *Permeable membranes having high flux-density and low fouling-propensity*. U.S. 4756835
(13) Yu, S. C.; Lu, Z. H.; Chen, Z. H.; Liu, X. S.; Liu, M. H.; Gao, C. J. *J. Membr. Sci.* **2011**, *371*, 293–306.
(14) Tang, C. Y. Y.; Kwon, Y. N.; Leckie, J. O. *J. Membr. Sci.* **2007**, *287*, 146–156.
(15) Tang, C. Y. Y.; Kwon, Y. N.; Leckie, J. O. *Desalination* **2009**, *242*, 168–182.
(16) Lee, S. Y.; Kim, H. J.; Patel, R.; Im, S. J.; Kim, J. H.; Min, B. R. *Polym. Adv. Technol.* **2007**, *18*, 562–568.
(17) Lee, H. S.; Im, S. J.; Kim, J. H.; Kim, H. J.; Kim, J. P.; Min, B. R. *Desalination* **2008**, *219*, 48–56.
(18) Lind, M. L.; Jeong, B. H.; Subramani, A.; Huang, X. F.; Hoek, E. M. V. *J. Mater. Res.* **2009**, *24*, 1624–1631.
(19) Kim, S. H.; Kwak, S. Y.; Sohn, B. H.; Park, T. H. *J. Membr. Sci.* **2003**, *211*, 157–165.

(20) Kwak, S. Y.; Kim, S. H.; Kim, S. S. *Environ. Sci. Technol.* **2001**, *35*, 2388–2394.
(21) Mo, J.; Son, S. H.; Jegal, J.; Kim, J.; Lee, Y. H. *J. Appl. Polym. Sci.* **2007**, *105*, 1267–1274.
(22) Mauter, M. S.; Elimelech, M. *Environ. Sci. Technol.* **2008**, *42*, 5843–5859.
(23) Vecitis, C. D.; Zodrow, K. R.; Kang, S.; Elimelech, M. *ACS Nano* **2010**, *4*, 5471–5479.
(24) Kang, S.; Mauter, M. S.; Elimelech, M. *Environ. Sci. Technol.* **2009**, *43*, 2648–2653.
(25) Choi, O. Y.; Yu, C. P.; Fernandez, G. E.; Hu, Z. Q. *Water Res.* **2010**, *44*, 6095–6103.
(26) Fabrega, J.; Fawcett, S. R.; Renshaw, J. C.; Lead, J. R. *Environ. Sci. Technol.* **2009**, *43*, 7285–7290.
(27) Hwang, E. T.; Lee, J. H.; Chae, Y. J.; Kim, Y. S.; Kim, B. C.; Sang, B. I.; Gu, M. B. *Small* **2008**, *4*, 746–750.
(28) Sotiriou, G. A.; Pratsinis, S. E. *Environ. Sci. Technol.* **2010**, *44*, 5649–5654.
(29) Tiraferri, A.; Yip, N. Y.; Phillip, W. A.; Schiffman, J. D.; Elimelech, M. *J. Membr. Sci.* **2011**, *367*, 340–352.
(30) Cai, L. T.; Bahr, J. L.; Yao, Y. X.; Tour, J. M. *Chem. Mater.* **2002**, *14*, 4235–4241.
(31) Chen, Z. Y.; Ziegler, K. J.; Shaver, J.; Hauge, R. H.; Smalley, R. E. *J. Phys. Chem. B* **2006**, *110*, 11624–11627.
(32) Simmons, J. M.; Nichols, B. M.; Baker, S. E.; Marcus, M. S.; Castellini, O. M.; Lee, C. S.; Hamers, R. J.; Eriksson, M. A. *J. Phys. Chem. B* **2006**, *110*, 7113–7118.
(33) Grabarek, Z.; Gergely, J. *Anal. Biochem.* **1990**, *185*, 131–135.
(34) Staros, J. V.; Wright, R. W.; Swingle, D. M. *Anal. Biochem.* **1986**, *156*, 220–222.
(35) Ghosh, A. K.; Jeong, B. H.; Huang, X. F.; Hoek, E. M. V. *J. Membr. Sci.* **2008**, *311*, 34–45.
(36) Wenzel, R. N. *J. Phys. Colloid Chem.* **1949**, *53*, 1466–1467.
(37) Schiffman, J. D.; Elimelech, M. *ACS Appl. Mater. Interfaces* **2011**, *3*, 462–468.
(38) Obrien, R. D.; Lindow, S. E. *Phytopathology* **1989**, *79*, 619–627.
(39) Upadhyayula, V. K. K.; Gadhamshetty, V. *Biotechnol. Adv.* **2010**.
(40) Kang, S.; Herzberg, M.; Rodrigues, D. F.; Elimelech, M. *Langmuir* **2008**, *24*, 6409–6413.
(41) Kang, S.; Pinault, M.; Pfefferle, L. D.; Elimelech, M. *Langmuir* **2007**, *23*, 8670–8673.
(42) Akdim, B.; Kar, T.; Duan, X. F.; Pachter, R. *Chem. Phys. Lett.* **2007**, *445*, 281–287.
(43) Li, M. H.; Boggs, M.; Beebe, T. P.; Huang, C. P. *Carbon* **2008**, *46*, 466–475.
(44) Dresselhaus, M. S.; Dresselhaus, G.; Saito, R.; Jorio, A. *Phys. Rep.—Rev. Sect. Phys. Lett.* **2005**, *409*, 47–99.
(45) Banerjee, S.; Wong, S. S. *Nano Lett.* **2004**, *4*, 1445–1450.
(46) Arepalli, S.; Nikolaev, P.; Gorelik, O.; Hadjiev, V. G.; Bradlev, H. A.; Holmes, W.; Files, B.; Yowell, L. *Carbon* **2004**, *42*, 1783–1791.
(47) Hemraj-Benny, T.; Bandosz, T. J.; Wong, S. S. *J. Colloid Interface Sci.* **2008**, *317*, 375–382.
(48) Obraztsova, E. A.; Lukashev, E. P.; Zarubina, A. P.; Parkhomenko, I. M.; Yaminsky, I. V. *Moscow Univ. Phys. Bull.* **2009**, *64*, 320–323.
(49) Wamser, C. C.; Gilbert, M. I. *Langmuir* **1992**, *8*, 1608–1614.
(50) Dhar, S.; Liu, Z.; Thomale, J.; Dai, H. J.; Lippard, S. J. *J. Am. Chem. Soc.* **2008**, *130*, 11467–11476.
(51) Hirsch, A.; Vostrowsky, O. *Func. Mol. Nanostruct.* **2005**, *245*, 193–237.
(52) Ma, H. Y.; Zhang, L. P.; Pan, Y.; Zhang, K. Y.; Zhang, Y. Z. *Electroanalysis* **2008**, *20*, 1220–1226.
(53) Ghaemy, M.; Mighani, H.; Behmadi, H. *J. Appl. Polym. Sci.* **2008**, *109*, 2388–2394.
(54) Marani, D.; Di Vona, M. L.; Traversa, E.; Licoccia, S.; Beurroies, I.; Llewellyn, P. L.; Knauth, P. *J. Phys. Chem. B* **2006**, *110*, 15817–15823.
(55) Zhang, X. G.; Loo, L. S. *Polymer* **2009**, *50*, 2643–2654.
(56) Mi, B. X.; Coronell, O.; Marinas, B. J.; Watanabe, F.; Cahill, D. G.; Petrov, I. *J. Membr. Sci.* **2006**, *282*, 71–81.